Letter

Solving the electronic structure problem for over 100 000 atoms in real space

Mehmet Dogan,[1] Kai-Hsin Liou,[2] and James R. Chelikowsky[1,2,3]
[1]*Center for Computational Materials, Oden Institute for Computational Engineering and Sciences, University of Texas at Austin, Austin, Texas 78712, USA*
[2]*McKetta Department of Chemical Engineering, University of Texas at Austin, Austin, Texas 78712, USA*
[3]*Department of Physics, University of Texas at Austin, Austin, Texas 78712, USA*

(Received 1 March 2023; revised 12 May 2023; accepted 1 June 2023; published 20 June 2023)

Using a real-space high-order finite-difference approach, we investigate the electronic structure of large spherical silicon nanoclusters. Within Kohn-Sham density functional theory and using pseudopotentials, we report the self-consistent field convergence of a system with over 100 000 atoms: a $Si_{107,641}H_{9,084}$ nanocluster with a diameter of 16 nm. Our approach uses Chebyshev-filtered subspace iteration to speed up the convergence of the eigenspace, and blockwise Hilbert space-filling curves to speed up sparse matrix-vector multiplications, all of which are implemented in the PARSEC code. For the largest system, we utilized 2048 nodes (114 688 cores) on the Frontera machine in the Texas Advanced Computing Center. Our quantitative analysis of the electronic structure shows how it gradually approaches its bulk counterpart as a function of nanocluster size. The band gap is enlarged due to quantum confinement in nanoclusters, but decreases as the system size increases, as expected. Our work serves as a proof of concept for the capacity of the real-space approach in efficiently parallelizing very large calculations using high-performance computer platforms, which can straightforwardly be replicated in other systems with more than 10^5 atoms.

DOI: 10.1103/PhysRevMaterials.7.L063001

Calculating the electronic structure of materials has been a primary aim for the theory of condensed matter physics, as well as the starting point for understanding and predicting materials properties. The development of density functional theory (DFT) [1,2] and pseudopotential methods [3] has made it possible to treat the problem as an effective one-electron problem, rather than the much more difficult interacting many-electron problem.

Over the past few decades, rapid improvements in computational capabilities allowed researchers to solve the electronic structure problem for larger and larger systems using various software packages. Currently, the most common available packages use a plane-wave basis in which to expand the Kohn-Sham wave functions. Despite the practical success of this approach, a few disadvantages exist: (1) the requirement of extensive global communications hindering massive parallelization; (2) the inability to directly calculate aperiodic structures such as nanoclusters and instead having to construct large supercells; and (3) the inability to calculate charged systems without a compensating background charge that might alter their properties.

An alternative approach utilizes a real-space grid to circumvent these shortcomings [4–7]. In our approach, which has been implemented in the software package PARSEC ("pseudopotential algorithm for real-space electronic structure calculations"), the Kohn-Sham equations are solved via high-order finite difference in real space [8,9]. The reduced need for global communication makes parallelization easier, and periodic simulation cells are not required (overcoming the latter two aforementioned issues), though they are also implemented. Various other implementations in real space have also been developed, e.g., multigrids [10–12], multiwavelets [13], finite-element [14–17], as well as other finite-difference implementations [18–23]. Achieving convergence within the finite-difference formalism is straightforward if the Coulomb singularity of the all electron potential is removed using pseudopotentials [24]. Additionally, the Hamiltonian matrices obtained on the real-space grid are large, but very sparse, enabling an efficient diagonalization [25].

Achieving self-consistency in large systems often involves handling a bottleneck associated with the solution of the eigenvalue problem. If there were a way to approximate the solution of the eigenvalue problem for the first few self-consistent field (SCF) steps without attempting full accuracy for individual eigenstates, that would result in a significant speedup. This idea has been realized by the Chebyshev-filtered subspace iteration (CheFSI). The focus of CheFSI is on improving the subspace (and as a result, the charge density) and the potentials simultaneously over successive SCF steps [26–29]. Rather than searching for individual eigenstates, the CheFSI method searches for an invariant subspace, which approaches the SCF eigensubspace. The CheFSI method provides a significant speedup (up to tenfold) compared to standard diagonalization techniques [26,29], which has led to its widespread use in real-space DFT packages [21–23,30,31]. The details of our current implementation of CheFSI in PARSEC can be found elsewhere [29].

The efficiency of the CheFSI method relies on sparse matrix-vector multiplications arising from the Hamiltonian and the wave functions. In order to parallelize these multiplications, one needs to partition the calculational domain and distribute calculations among processors, which has the potential of being very inefficient when thousands of processors are involved. We have recently investigated the most

TABLE I. The silicon NCs studied in this Letter. For each system, the corresponding grid spacing (h), the machine on which the calculation was run, the number of computing nodes, the diameter of the NC, the number of grid points, the number of computed states, the number of SCF steps to reach convergence, and the wall time for the calculation are tabulated.

	h (bohr)	Machine	No. of nodes	Diameter (nm)	No. of grid points	No. of states	No. of SCF steps	Wall time (h)
$Si_{1,947}H_{604}$	0.7	Cori	2	4.2	1,575,600	4800	17	2.5
$Si_{4,001}H_{1,012}$	0.7	Cori	8	5.3	2,707,504	9216	19	4.0
$Si_{10,869}H_{1,924}$	0.7	Cori	64	7.5	6,377,184	24,576	17	8.4
$Si_{23,049}H_{3,220}$	0.7	Cori	256	9.6	15,180,904	61,440	18	27.9
$Si_{51,071}H_{5,484}$	0.9	Frontera	512	12.5	15,522,368	114,688	15	28.6
$Si_{107,641}H_{9,084}$	0.9	Frontera	2048	16.0	31,901,640	245,760	14	46.8

efficient ways of domain partitioning based on space-filling curves (SFCs) [32]. SFCs are continuous curves that traverse a three-dimensional (3D) domain and pass through every grid point once. This presents a straightforward way to access data on each point, while the self-similarity of SFCs preserves the locality of the grid points on the curve [33–36]. We have found that using blockwise Hilbert SFCs can provide an over sixfold speedup of sparse matrix-vector multiplications compared to simple Cartesian ordering [32].

Here, we present a large Kohn-Sham DFT calculation with SCF convergence (a silicon nanocluster made up of over 100 000 atoms or 400 000 electrons) using the Chebyshev-filtered subspace iteration and blockwise Hilbert space-filling curves implemented in the real-space code PARSEC. We also compare this system ($Si_{107,641}H_{9,084}$) to smaller nanoclusters to investigate the evolution of the electronic structure as a function of the system size. This achievement demonstrates the robust scalability and parallelizability of the real-space method.

The calculations presented here were run on two supercomputers: the National Energy Research Scientific Computing Center's (NERSC) Cori machine, and the Texas Advanced Computing Center's (TACC) Frontera machine. On Cori, we used Knights Landing (KNL) nodes, each of which is equipped with one Intel Xeon Phi 7250 processor, which has 68 CPU cores. On Frontera, each node is equipped with two Intel Xeon Platinum 8280 processors and has 56 CPU cores. We used norm-conserving pseudopotentials, constructed by the Troullier-Martins method in the Kleimann-Bylander form [37,38]. The cutoff radii for hydrogen and silicon atoms are 1.8 bohrs for $1s^1$ and 2.78 bohrs for $3s^2$, $3p^2$, and $3d^0$, respectively. We employed the local density approximation (LDA) to approximate the exchange-correlation functional as determined numerically by Ceperley and Alder [39], and parametrized by Perdew and Zunger [40]. We note that some newly developed functionals such as meta-GGA (generalized gradient approximation) can provide more accurate energy gaps without sacrificing the calculation speed, and thus for future simulations concerned with comparisons with optical experiments, those functionals can be used [41,42]. We applied four iterations of CheFSI during the first SCF step, and then one iteration for each following step. Our SCF convergence criterion is SRE < 0.0001 Ry, where SRE (self-consistent residual error) is defined as the integral of the square of the difference between the last two self-consistent potentials, weighted by electron density and taken squared root. All further details regarding the CheFSI algorithm can be found in Refs. [25,29,32].

We list and summarize the calculations we ran in Table I. Each calculation is a spherical silicon nanocluster (NC) generated from bulk silicon in the diamond crystal structure with the optimized lattice constant 5.38 Å, within 1% of the observed lattice constant of 5.43 Å. The dangling bonds of the surface silicons are passivated by hydrogen atoms. Among the six NCs listed, the second, third, and fourth ones were previously reported in Ref. [32], and are included here for comparison. For the larger NCs ($Si_{51,071}H_{5,484}$ and $Si_{107,641}H_{9,084}$), we switched from the Cori machine to the Frontera machine, which has a higher clock rate (2.7 GHz vs 1.4 GHz) and memory per node (192 GB vs 96 GB). For these NCs, we also increased the grid spacing h from 0.7 bohrs to 0.9 bohrs, which reduced the problem size by a factor of $(0.7/0.9)^3 \simeq 0.47$. We have verified for the smaller NCs that the grid spacing of 0.9 bohrs leads to well-converged eigenvalues for the energy spectrum, leading to histograms of energies hardly distinguishable from those resulting from $h = 0.7$ bohrs. As an example, the as-computed eigenvalues for highest occupied molecular orbital (HOMO) and lowest unoccupied molecular orbital (LUMO) states for $Si_{1,947}H_{604}$ are -4.9997 (-5.0031) eV and -4.0459 (-4.0508) eV for $h = 0.7$ (0.9) bohrs. We note that the largest NC studied here required the use of 2048 nodes (114 688 cores), which corresponds to a quarter of the full Frontera capacity. In comparison, the only other Kohn-Sham DFT calculation of a similar size to our knowledge, which is a single SCF steps on a 107 292-atom silicon nanowire (also utilizing high-order finite-difference real-space methods) was achieved using 442 384 cores on the K Computer at Riken Advanced Institute for Computational Science [43]. A more recent attempt at a very large calculation was of a $\sim$10 000 atom Mg system with $\sim$100 000 electrons, using 3800 GPU nodes on the Summit Supercomputer at Oak Ridge Leadership Computing Facility. This study utilized a real-space finite-element method [44].

In real space, each state is a function of space in the whole calculation domain. Therefore, the total number of degrees of freedom in our largest calculation is 7.8×10^{12} (computed as No. of grid points $\times$ No. of states read off Table I). The fact that the Hamiltonian is sparse and we are only computing a small low-energy subset of the eigenspace (0.77% of the total number of eigenstates) greatly helps in making this problem more tractable [45].

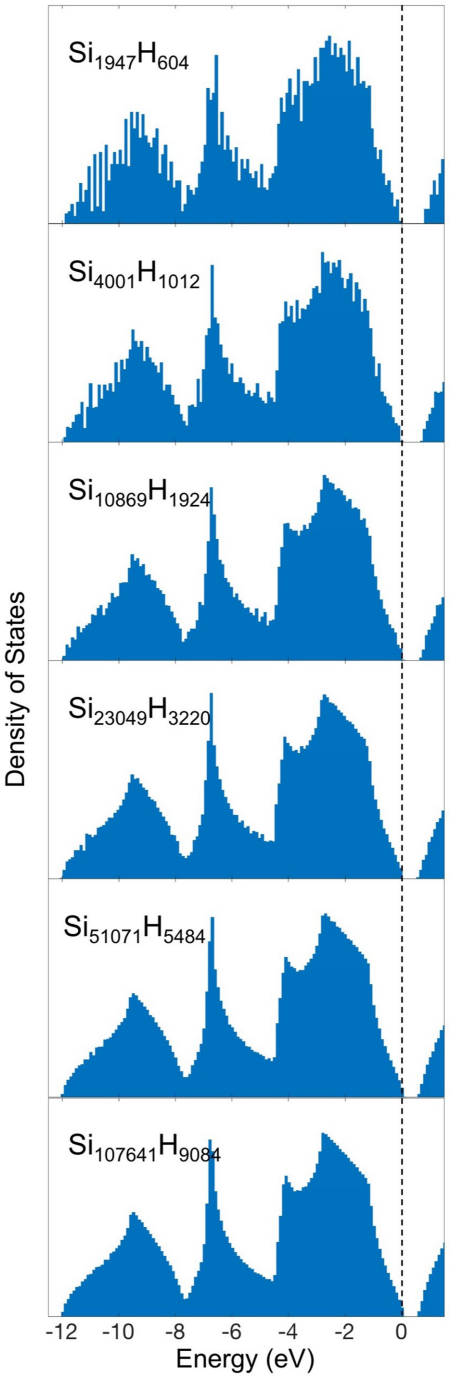

FIG. 1. The density of states (DOS) for the six NCs investigated in this Letter. The DOS for each case is obtained by plotting a histogram of the eigenstates using 0.1 eV bins. The highest occupied state (Fermi level) is set to zero in each case.

We present the density of states computed for each of the six NCs in Fig. 1. In order to plot the DOS for a given system, we first set the eigenvalue for the highest occupied state (Fermi level) to zero, then create a histogram of eigenvalues using 0.1 eV bins, and finally normalize each plot so that they all have the same total area below the Fermi level. We observe that as the NC gets larger, the DOS becomes less "noisy," and the familiar features of the bulk DOS become more discernible. The dip around −8 eV and the van Hove singularity around −7 eV become sharper for larger NCs [46]. We note that these sharp features which can be understood in the context of band theory nevertheless arise in our real-space calculation which does not invoke Bloch's theorem.

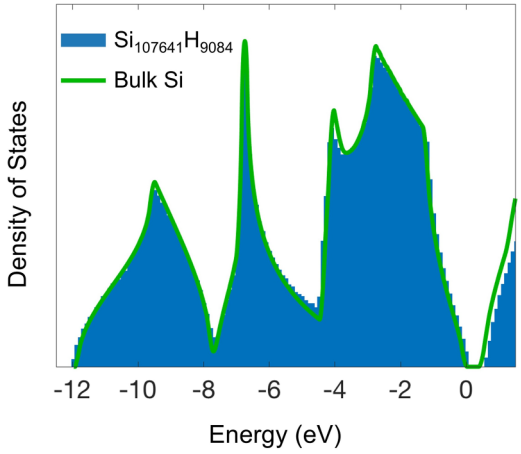

FIG. 2. The density of states (DOS) for the $Si_{107,641}H_{9,084}$ NC (blue bars) plotted together with the DOS of bulk silicon (green line), both obtained from PARSEC using similar grid spacings. The NC DOS is obtained by plotting a histogram of the eigenstates using 0.1 eV bins, and then normalized to match the area under the valence-band part of the bulk Si curve. The highest occupied state of the NC is set to zero, and the valence-band edge of the bulk DOS is positioned to minimize the rms difference between the two plots.

In order to systematically study how the electronic structure of the NCs converge to the bulk, we performed a bulk silicon calculation in PARSEC with $h = 0.86$ bohr using the periodic boundary conditions [7,47]. and a $36 \times 36 \times 36$ Monkhorst-Pack k-point sampling for the 8-atom simple cubic cell [48]. To compare the bulk DOS and the DOS of the $Si_{107,641}H_{9,084}$ NC, we first sample the bulk DOS on the same energy values that are used to generate the DOS of the NC. We then normalize the DOS of the NC such that the total area under the valence-band part is equal to the bulk counterpart. We then calculate the root mean square (rms) of the difference between the two curves, which we self-consistently minimize by horizontally shifting the bulk DOS plot. The resulting comparison with a minimized rms is presented in Fig. 2. All features of the bulk DOS are replicated in the NC DOS with high precision. The deviation at the conduction-band edge is an expected result of quantum confinement.

By repeating the same analysis for the smaller NCs, we have obtained Fig. 3, which shows the evolution of the band gap and the rms deviation for each DOS from the bulk DOS. We observe that the deviation from bulk electronic structure monotonically decreases with the size of the NC, the decrease being sharper up to ∼10 nm. The evolution of the band gap (HOMO-LUMO gap) follows a power law, in accordance with previous studies on quantum confinement [27,49–54]. By fitting the band gap versus diameter d to the expected equation, we find

$$E_{\mathrm{gap}}(d) = 0.46\ \mathrm{eV} + \frac{4.64}{(d\ \mathrm{in\ nm})^{1.56}}\ \mathrm{eV},$$

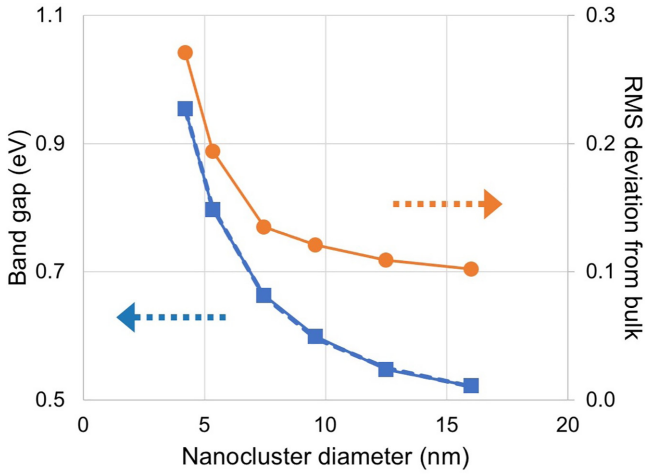

FIG. 3. The evolution of the band gap and the rms deviation for each DOS from the bulk DOS for the six computed silicon NCs considered in this Letter. The blue curve with square marks plots the band gap (left axis), and the orange curve with round marks plots the rms deviation from the bulk DOS (right axis). A best fit curve with a power-law dependence and a vertical offset is also included for the band-gap curve (dashed). The fit has $R^2 = 0.9998$.

with a coefficient of determination of 0.9998 (plotted with a blue dashed line in Fig. 3). The 0.46 eV value also agrees with the band gap computed in our bulk Si calculation. Previous studies into smaller Si NCs have found smaller exponents (between 1.08 and 1.39) [27,51–53]. The fact that our exponent is larger is in agreement with the expectation that in the bulk limit, the effective mass theory of quantum confinement becomes valid, and the exponent approaches 2 [49–51].

As we previously mentioned, the real-space approach is suitable for computing charged systems [55]. This allows us to compare the HOMO-LUMO gap and the fundamental gap, defined as the difference between the ionization potential $[E_{\text{total}}(n) - E_{\text{total}}(n-1)]$ and electron affinity $[E_{\text{total}}(n+1) - E_{\text{total}}(n)]$, where n is the number of electrons in the neutral NC. In a previous study, we studied the evolution of these two gaps for NCs up to a diameter of 7.0 nm ($Si_{9,041}H_{1,860}$) [27], finding the fundamental gap for the largest NC to be 1.54 eV and the HOMO-LUMO gap to be 0.97 eV. In this Letter, we have repeated these calculations for $d = 7.5$ nm ($Si_{10,869}H_{1,924}$) and $d = 9.6$ nm ($Si_{23,049}H_{3,220}$). We find the fundamental gap for these NCs to be 1.53 and 1.33 eV, respectively, and the HOMO-LUMO gap to be 0.96 and 0.80 eV, respectively. Therefore, the difference between these two gaps goes from 0.57 to 0.53 eV from the smaller NC to the larger NC, which is in line with the results from our previous study [27].

In summary, we have presented the successful SCF convergence of one of the largest systems to date ($Si_{107,641}H_{9,084}$ nanocluster with a diameter of 16 nm) in Kohn-Sham density functional theory, achieved using a real-space finite-difference approach implemented in the PARSEC code. Our method utilizes Chebyshev-filtered subspace iteration to speed up the convergence of the eigenspace, and blockwise Hilbert space-filling curves to speed up sparse matrix-vector multiplications. For this Letter, we executed highly parallelized runs with up to 2048 nodes (114 688 cores) on TACC Frontera. We have also systematically investigated the convergence of the electronic structure into its bulk counterpart as a function of the nanocluster size. We have confirmed the predicted behavior of the band gap as it is enlarged due to quantum confinement in nanoclusters. Our work demonstrates the capabilities of the real-space approach in achieving a very high level of parallelization in modern supercomputers, delivering accurate electronic structure results in unprecedented system sizes. As our supercomputers continue to improve into the so-called exascale era, the ever-growing electronic structure community needs software that can scale up and meet the challenge. We have shown that fully *ab initio* calculations in the ($\sim$10 nm^3) scale can now be done, which will pave the way for further applications in the exascale era.

M.D. acknowledges support from the "Characteristic Science Applications for the Leadership Class Computing Facility" project, which is supported by National Science Foundation Award No. 2139536. J.R.C. and K.H.L. acknowledge support by a subaward from the Center for Computational Study of Excited-State Phenomena in Energy Materials (C2SEPEM) at the Lawrence Berkeley National Laboratory, which is funded by the U.S. Department of Energy under Contract No. DE-AC02- 05CH11231, as part of the Computational Materials Sciences Program. Computational resources are provided by the National Energy Research Scientific Computing Center (NERSC) as well as the Texas Advanced Computing Center (TACC). J.R.C. also acknowledges support from the Welch Foundation under Grant No. F-2094. We thank Dr. Junjie Li from TACC for technical support.

[1] P. Hohenberg and W. Kohn, Phys. Rev. **136**, B864 (1964).
[2] W. Kohn and L. J. Sham, Phys. Rev. **140**, A1133 (1965).
[3] J. R. Chelikowsky and M. L. Cohen, Ab initio pseudopotentials and the structural properties of semiconductors, *Basic Properties of Semiconductors*, Handbook on Semiconductors (Elsevier, Amsterdam, 1992), pp. 59–112.
[4] J. R. Chelikowsky, N. Troullier, and Y. Saad, Phys. Rev. Lett. **72**, 1240 (1994).
[5] A. Stathopoulos, S. Ogut, Y. Saad, J. Chelikowsky, and H. Kim, Comput. Sci. Eng. **2**, 19 (2000).
[6] J. R. Chelikowsky, L. Kronik, I. Vasiliev, M. Jain, and Y. Saad, Using real space pseudopotentials for the electronic structure problem, Handbook of Numerical Analysis, Special Volume, Computational Chemistry (Elsevier, Amsterdam, 2003), Vol. 10, pp. 613–637.
[7] M. M. G. Alemany, M. Jain, L. Kronik, and J. R. Chelikowsky, Phys. Rev. B **69**, 075101 (2004).
[8] L. Kronik, A. Makmal, M. L. Tiago, M. M. G. Alemany, M. Jain, X. Huang, Y. Saad, and J. R. Chelikowsky, Phys. Status Solidi B **243**, 1063 (2006).

[9] V. Gavini, S. Baroni, V. Blum, D. R. Bowler, A. Buccheri, J. R. Chelikowsky, S. Das, W. Dawson, P. Delugas, M. Dogan, C. Draxl, G. Galli, L. Genovese, P. Giannozzi, M. Giantomassi, X. Gonze, M. Govoni, A. Gulans, F. Gygi, J. M. Herbert *et al.*, arXiv:2209.12747.

[10] J. Bernholc, M. Hodak, and W. Lu, J. Phys.: Condens. Matter **20**, 294205 (2008).

[11] O. Cohen, L. Kronik, and A. Brandt, J. Chem. Theory Comput. **9**, 4744 (2013).

[12] J. Zhang, Y. Cheng, W. Lu, E. Briggs, A. J. Ramirez-Cuesta, and J. Bernholc, J. Chem. Theory Comput. **15**, 6859 (2019).

[13] S. R. Jensen, S. Saha, J. A. Flores-Livas, W. Huhn, V. Blum, S. Goedecker, and L. Frediani, J. Phys. Chem. Lett. **8**, 1449 (2017).

[14] J. E. Pask, B. M. Klein, P. A. Sterne, and C. Y. Fong, Comput. Phys. Commun. **135**, 1 (2001).

[15] B. Kanungo and V. Gavini, Phys. Rev. B **100**, 115148 (2019).

[16] P. Motamarri, S. Das, S. Rudraraju, K. Ghosh, D. Davydov, and V. Gavini, Comput. Phys. Commun. **246**, 106853 (2020).

[17] S. Das, P. Motamarri, V. Subramanian, D. M. Rogers, and V. Gavini, Comput. Phys. Commun. **280**, 108473 (2022).

[18] J.-I. Iwata, D. Takahashi, A. Oshiyama, T. Boku, K. Shiraishi, S. Okada, and K. Yabana, J. Comput. Phys. **229**, 2339 (2010).

[19] X. Andrade, D. Strubbe, U. D. Giovannini, A. H. Larsen, M. J. T. Oliveira, J. Alberdi-Rodriguez, A. Varas, I. Theophilou, N. Helbig, M. J. Verstraete, L. Stella, F. Nogueira, A. Aspuru-Guzik, A. Castro, M. A. L. Marques, and A. Rubio, Phys. Chem. Chem. Phys. **17**, 31371 (2015).

[20] W. Mi, X. Shao, C. Su, Y. Zhou, S. Zhang, Q. Li, H. Wang, L. Zhang, M. Miao, Y. Wang, and Y. Ma, Comput. Phys. Commun. **200**, 87 (2016).

[21] V. Michaud-Rioux, L. Zhang, and H. Guo, J. Comput. Phys. **307**, 593 (2016).

[22] S. Ghosh and P. Suryanarayana, Comput. Phys. Commun. **212**, 189 (2017).

[23] S. Ghosh and P. Suryanarayana, Comput. Phys. Commun. **216**, 109 (2017).

[24] J. R. Chelikowsky, J. Phys. D **33**, R33 (2000).

[25] Y. Saad, J. R. Chelikowsky, and S. M. Shontz, SIAM Rev. **52**, 3 (2010).

[26] Y. Zhou, Y. Saad, M. L. Tiago, and J. R. Chelikowsky, Phys. Rev. E **74**, 066704 (2006).

[27] J. R. Chelikowsky, M. L. Tiago, Y. Saad, and Y. Zhou, Comput. Phys. Commun. **177**, 1 (2007).

[28] Y. Zhou, J. R. Chelikowsky, and Y. Saad, J. Comput. Phys. **274**, 770 (2014).

[29] K.-H. Liou, C. Yang, and J. R. Chelikowsky, Comput. Phys. Commun. **254**, 107330 (2020).

[30] B. Kanungo and V. Gavini, Phys. Rev. B **95**, 035112 (2017).

[31] A. S. Banerjee, L. Lin, P. Suryanarayana, C. Yang, and J. E. Pask, J. Chem. Theory Comput. **14**, 2930 (2018).

[32] K.-H. Liou, A. Biller, L. Kronik, and J. R. Chelikowsky, J. Chem. Theory Comput. **17**, 4039 (2021).

[33] J. K. Lawder and P. J. H. King, in *Advances in Databases*, edited by B. Lings and K. Jeffery, Lecture Notes in Computer Science (Springer, Berlin, 2000), pp. 20–35.

[34] B. Moon, H. Jagadish, C. Faloutsos, and J. Saltz, IEEE Trans. Knowl. Data Eng. **13**, 124 (2001).

[35] A.-J. N. Yzelman and D. Roose, IEEE Trans. Parallel Distrib. Syst. **25**, 116 (2014).

[36] P. Xu and S. Tirthapura, ACM Trans. Database Syst. **39**, 10 (2014).

[37] N. Troullier and J. L. Martins, Phys. Rev. B **43**, 1993 (1991).

[38] L. Kleinman and D. M. Bylander, Phys. Rev. Lett. **48**, 1425 (1982).

[39] D. M. Ceperley and B. J. Alder, Phys. Rev. Lett. **45**, 566 (1980).

[40] J. P. Perdew and A. Zunger, Phys. Rev. B **23**, 5048 (1981).

[41] T. Aschebrock and S. Kümmel, Phys. Rev. Res. **1**, 033082 (2019).

[42] P. Borlido, J. Schmidt, A. W. Huran, F. Tran, M. A. L. Marques, and S. Botti, npj Comput. Mater. **6**, 96 (2020).

[43] Y. Hasegawa, J.-I. Iwata, M. Tsuji, D. Takahashi, A. Oshiyama, K. Minami, T. Boku, F. Shoji, A. Uno, M. Kurokawa, H. Inoue, I. Miyoshi, and M. Yokokawa, *Proceedings of the 2011 International Conference for High Performance Computing, Networking, Storage and Analysis, SC'11* (Association for Computing Machinery, New York, 2011), Article 1, pp. 1–11.

[44] S. Das, P. Motamarri, V. Gavini, B. Turcksin, Y. W. Li, and B. Leback, *Proceedings of the 2019 International Conference for High Performance Computing, Networking, Storage and Analysis, SCrapos;19* (Association for Computing Machinery, New York, 2019), Article 2, pp. 1–11.

[45] G. Schofield, J. R. Chelikowsky, and Y. Saad, Comput. Phys. Commun. **183**, 497 (2012).

[46] M. L. Cohen and J. R. Chelikowsky, *Electronic Structure and Optical Properties of Semiconductors*, Springer Series in Solid-State Sciences No. 75 (Springer, Berlin, 1988).

[47] A. Natan, A. Benjamini, D. Naveh, L. Kronik, M. L. Tiago, S. P. Beckman, and J. R. Chelikowsky, Phys. Rev. B **78**, 075109 (2008).

[48] H. J. Monkhorst and J. D. Pack, Phys. Rev. B **13**, 5188 (1976).

[49] L. E. Brus, J. Chem. Phys. **80**, 4403 (1984).

[50] L. Brus, J. Phys. Chem. **90**, 2555 (1986).

[51] C. Delerue, G. Allan, and M. Lannoo, Phys. Rev. B **48**, 11024 (1993).

[52] S. Öğüt, J. R. Chelikowsky, and S. G. Louie, Phys. Rev. Lett. **79**, 1770 (1997).

[53] V. Kocevski, O. Eriksson, and J. Rusz, Phys. Rev. B **87**, 245401 (2013).

[54] E. G. Barbagiovanni, D. J. Lockwood, P. J. Simpson, and L. V. Goncharova, Appl. Phys. Rev. **1**, 011302 (2014).

[55] T. Liao, K.-H. Liou, and J. R. Chelikowsky, Phys. Rev. Mater. **6**, 054603 (2022).